Advances in Water Resources 67 (2014) 78–86

Contents lists available at ScienceDirect

Advances in Water Resources

journal homepage: www.elsevier.com/locate/advwatres

A fractal model to describe the evolution of multiphase flow properties during mineral dissolution

Luis Guarracino [a], Tobias Rötting [b,c,*], Jesus Carrera [c]

[a] CONICET, Facultad de Ciencias Astronómicas y Geofísicas, Universidad Nacional de La Plata, Paseo del Bosque s/n, 1900 La Plata, Argentina
[b] Department of Geotechnical Engineering and Geo-Sciences, Technical University of Catalonia (UPC Barcelona Tech), c/ Jordi Girona 1-3, 08034 Barcelona, Spain
[c] Department of Geosciences, Institute of Environmental Assessment and Water Research (IDAEA), Spanish National Research Council (CSIC), c/ Jordi Girona 18, 08034 Barcelona, Spain

ARTICLE INFO

Article history:
Received 2 March 2013
Received in revised form 24 February 2014
Accepted 25 February 2014
Available online 4 March 2014

Keywords:
Fractal model
Multiphase flow
Pore size distribution
Water retention curve
Diffusion
Dissolution
Representative elementary volume

ABSTRACT

Understanding the changes in multiphase flow parameters caused by mineral dissolution-precipitation is required for multiple applications ranging from geological storage of CO_2, enhanced geothermal energy production or ground water pollution. We present a physically-based theoretical model for describing the temporal evolution of porosity, saturated and relative permeabilities, retention curve and diffusion coefficient during rock dissolution by reactive fluids. The derivation of the model is based on the assumption that the pore structure of the rock can be represented by an ensemble of capillary tubes with fractal tortuosity and cumulative pore size distribution. Therefore, the model depends only on the minimum and maximum pore radii, the size of the representative elementary volume and the fractal dimensions of pore size and tortuosity, but do not need any other fitting parameters. Using this fractal description and known physical properties, we obtain analytical expressions for the hydrodynamic properties required by continuum (i.e., Darcy scale) multiphase flow models. Further, assuming periodic fluctuations in the radius of the pores, it is also possible to represent constrictivity and hysteresis. Finally, assuming a constant rate dissolution reaction it is possible to derive closed-form analytical expressions for the time evolution of porosity, retention curve, saturated and relative permeabilities and diffusion coefficient.

1. Introduction

Mineral dissolution or precipitation may play an important role in many vadose zone and multiphase flow processes. These include the geological storage of carbon dioxide, enhanced oil or gas recovery, flow and transport in unsaturated soil, geothermal systems, etc. (e.g., [1], and citations therein). Modelling these phenomena is most frequently achieved at the continuum (Darcy) scale, which requires specifying macroscale parameters, such as porosity, saturated and relative permeabilities, retention curve and molecular diffusion coefficient. Mineral precipitation or dissolution caused by the flow of a reactive fluid produces volume and surface variations at the pore level that are translated into variations of the multiphase flow and transport properties at the macroscale (e.g., [2]). The characterization of these parameters and constitutive relationships is therefore essential for adequate understanding and modelling of the transport of reactive substances.

Most published studies on dissolution processes in porous media concentrate on the changes of porosity and saturated liquid permeability (e.g., [3]), while relationships with or between the other multiphase flow parameters have been investigated less intensively. The most widely used approach relates saturated permeability to porosity via a power law $K \propto \phi^n$. It can be derived from the equations of Kozeny [4] and Carman [5], which leads to an exponent n equal to 3. Later works, e.g., [6–9], showed that this exponent can actually vary considerably depending on the type of porous medium and the flow and transport conditions. In some cases, exponents greater than 10 [6] or even 100 [9] have been found experimentally, particularly when preferential flow paths or "wormholes" were developing in previously homogeneous and isotropic media. These relationships have been applied extensively (see [10] for a review), but they have been derived for saturated conditions and are not linked to the other multiphase flow parameters.

Two families of models can be identified that have the potential to simulate the impact of dissolution on multiphase flow parameters: Pore scale models and bundles of tubes.

Pore scale models are based on simulating flow, transport and chemical reactions at the microscale (e.g., [11–14]). In a recent

* Corresponding author at: Department of Geotechnical Engineering and Geo-Sciences, Technical University of Catalonia (UPC Barcelona Tech), c/ Jordi Girona 1-3, 08034 Barcelona, Spain. Tel.: +34 653217596.
E-mail address: tobias.roetting@upc.edu (T. Rötting).

http://dx.doi.org/10.1016/j.advwatres.2014.02.011
0309-1708/

review, Meakin and Tartakovsky [14] stated that well-developed methods are available to represent saturated subsurface flow systems at the pore-scale. In practice, this is difficult, even for single phase, because it requires a detailed description of the porous structure, but it is feasible. However, the simulation of multiphase systems is much more challenging due to potentially large density or viscosity ratios of contacting fluids, and the complex behaviour of fluid-fluid-solid contact lines and their impact on dynamic contact angles. Pore-scale models can represent dissolution or precipitation and their impact on fluid flow (e.g., [15–18]). Moreover, hybrid models and other upscaling approaches have been developed for combining micro- and macroscale descriptions in order to study larger (Darcy or field) scale problems (e.g., [19–22]). However, by requiring an image of the pore space and the link between pore network and continuum scale equations, these models appear to be too complex for a widespread application in the near future.

The porous medium can also be represented by bundles of tubes to derive macroscale continuum properties. Contrary to pore network models, bundles of tubes imply perfect pore connectivity. As such, they cannot yield multicontinuum descriptions of the medium, which can be achieved with pore network models (e.g., [23–25]). The motivation of bundles of tubes lies on their simplicity. In fact, many empirical models have been developed and widely used for predicting relative permeability and retention curve assuming different pore size distributions (e.g., [26–29]). More recently, fractal distribution has often been adopted to describe the distribution of pore or particle sizes. They are based on the assumption that the soil solid phase, the soil void space or both display self-similarity (e.g., [30–33]). Tyler and Wheatcraft [33] described the soil pore size distribution using the Sierpinski Carpet [34] to develop a power-law form for the retention curve, equivalent to the functions of Brooks and Corey [26] and Campbell [35]. The Sierpinski Carpet has been also used to derive constitutive models for unsaturated flow in fractured rocks [36,37].

Fractal models of soil mass, pore volume and surface, fragmentation, soil-water retention and unsaturated hydraulic conductivity were reviewed and compared by Gimenez et al. [38] and Ghanbarian-Alavijeh et al. [39], but none of these approaches are capable of representing dissolution processes, hysteresis or diffusion.

Actual changes in hydrologic properties of aquifer media caused by chemical reactions are reviewed by Saripalli et al. [2]. They cite many different approaches to represent these changes in saturated media, i.e. geochemical equilibrium and kinetic models, chemical divide pathway models, flow and transport models, precipitation/dissolution wave theory, network models, porosity and permeability reduction models. However, they did not find any fractal approaches to model these changes, nor methods for unsaturated media or multiphase flow problems. More recently, several approaches have been proposed to model changes in porosity and permeability due to chemical reactions. Bartels et al. [40] combined the fractal porosity-permeability relationship of Pape et al. [6] with a numerical reactive transport code to calculate permeability changes in hydrogeothermal problems under fully saturated conditions from the change of bulk porosity. Freedman et al. [41] developed a film depositional model of permeability for mineral reactions in unsaturated media. They assumed that, even at partial saturation, reactions and volumetric changes occur throughout the entire pore-size distribution, and that the shape of the pore-size distribution would remain the same. Wissmeier and Barry [42] developed a selective radius shift model to describe the effect of mineral reactions on the hydraulic properties of unsaturated soils. In their model, reactions occur and pore radii change only in the smaller, water filled pores.

Hysteresis in the capillary pressure curve, i.e. the differences in water content at the same matric potential during drying and wetting, occurs due to contact angle effects, entrapped air, swelling and shrinking, and inkbottle effects, i.e. pores with narrow necks and wider bodies (e.g., [43]). Soil water hysteresis has been described using several approaches [44]: modelling by empirical and semi-empirical synthetic formulae, percolation theory, thermodynamic theory, fractal approach and domain theory. Details on many of the non-fractal approaches can be found in recent reviews [45–47]. Ojeda et al. [48] developed an early fractal model to describe hysteresis by defining a piecewise water-retention curve. Perfect [49] proposed a closed-form expression to describe the primary drainage curve of prefractal porous media. Russell and Buzzi [47] described the pores as a piecewise succession of bodies and throats and defined fractal distributions of body or throat sizes, which allowed them to describe the hysteretic loop observed during a drying–wetting–drying cycle.

Diffusion coefficients in porous media have been predicted from porosity (e.g., [50,51]) analogous to Archie's law [52]. Similar exponential relationships have also been derived experimentally [53] or using fractal approaches [54]. Analytical solutions for diffusion problems with precipitation-dissolution reactions were derived by Hayek et al. [55]. A method to predict diffusion coefficients from interfacial areas in unsaturated media represented by tortuous pore bundles was developed by Saripalli et al. [56].

From the above, it is clear that considerable advances have been achieved in the modelling of each of the processes involved in multiphase flow and reactive transport. However, no model is available that links all the involved parameters, which is a pre-requisite for modelling how these parameters change in response to changes in the pore structure caused by chemical reactions.

The objective of this work is to derive a physically-based model that describes saturated and relative permeabilities, porosity, retention curve and molecular diffusivity of a porous medium and how they change in response to dissolution processes. To this end, all these properties are obtained in terms of a fractal pore-size and tortuosity distribution, maximum and minimum radii of pores, and the size of the representative elementary volume (REV). We then present a simple theoretical model to predict the temporal evolution of these properties in response to dissolution of the solid matrix. In this model the rock is described as an impermeable matrix with cylindrical circular pores whose sizes follow a fractal distribution law. By assuming periodic fluctuations in the radius of the pores, it is possible to represent hysteresis in the retention curve and in the relative permeability function. The porous medium is then assumed to be dissolved by a fluid that reacts uniformly with the surface of the pores and that this process is far from local chemical equilibrium. We apply a function that describes the variation of the pore radii caused by dissolution or precipitation to derive continuous closed-form analytical expressions for the temporal evolution of the parameters and constitutive relationships that can be easily implemented into continuum-scale reactive transport codes.

2. Constitutive model

The rock matrix is conceptualized as an equivalent bundle of tortuous capillary tubes with a fractal law distribution of pore sizes [33,57,58]. The REV is assumed to be a straight circular cylinder of radius R and length L.

The pore structure of the REV is represented by an ensemble of tubes with periodically varying aperture, as illustrated in Fig. 1. The pore radius is described by the following sinusoidal function (similar to Czachor [59] and references therein):

$$r(x) = \overline{r} + r' \sin(2\pi x/\lambda) = \overline{r}(1 + 2a \sin(2\pi x/\lambda)) \quad (1)$$

where $\overline{r}$ is the average radius, r' the amplitude of the fluctuation, λ the wavelength, and a the fluctuation ratio defined by $a = r'/2\overline{r}$ with

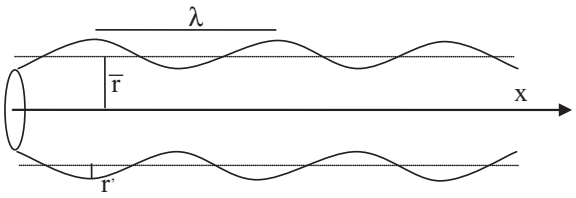

Fig. 1. Pore geometry.

$0 \leqslant a < 0.5$. Notice that x is measured along the pore length, which would only equal the dimension along the REV for straight tubes.

The cumulative size-distribution of pores whose average radii are greater than or equal to $\bar{r}$ is assumed to obey the following fractal scaling law [33,57,58]:

$$N(\bar{r}) = \left(\frac{\bar{r}_{\max}}{\bar{r}}\right)^{D_p} \tag{2}$$

where D_p is the fractal dimension of pore size ($0 < D_p < 2$) and $\bar{r}_{\max}$ is the maximum average radius of pores. Then, differentiating (2) with respect to $\bar{r}$ we obtain the number of pores whose average radii are in the infinitesimal range $\bar{r}$ to $\bar{r} + d\bar{r}$:

$$dN = -D_p \bar{r}_{\max}^{D_p} \bar{r}^{-D_p-1} d\bar{r} \tag{3}$$

The fractal tortuous length of tubes is described by the fractal scaling law of Wheatcraft and Tyler [60], who write it in terms of a scaling factor (length of measurement along the tortuous path). We set equal the scaling factor equal to the average pore radius, so that the tube length becomes

$$l(\bar{r}) = \bar{r}^{1-D_t} L^{D_t} = L(L/\bar{r})^{D_t-1} \tag{4}$$

where D_t is the tortuosity fractal dimension, with $1 < D_t < 2$. Note that the limiting cases $D_t = 1$ and $D_t = 2$ represent a straight tube and a highly tortuous tube that fills a plane, respectively. The right most expression implies that the tortuosity of each tube $[\tau = (L/\bar{r})^{D_t-1}]$ increases with decreasing average pore radius, $\bar{r}$.

2.1. Porosity

The volume of a single tube can be obtained by integrating the cross-sectional area over the tortuous length $l(\bar{r})$

$$V_p = \int_0^{l(\bar{r})} \pi [r(x)]^2 dx \tag{5}$$

According to (1) and (4), and assuming $\lambda \ll l(\bar{r})$, the volume V_p defined by (5) can be expressed as

$$V_p(\bar{r}) = \pi \bar{r}^{3-D_t} L^{D_t} [1 + 2a^2] \tag{6}$$

According to the definition of porosity we have

$$\phi = \frac{\int_{\bar{r}_{\min}}^{\bar{r}_{\max}} V_p(\bar{r})\, dN}{\pi R^2 L} \tag{7}$$

Finally, replacing (3) and (6) into (7) yields

$$\phi = \frac{L^{D_t-1}(1 + 2a^2) D_p \bar{r}_{\max}^{D_p}}{R^2 (3 - D_p - D_t)} \left[\bar{r}_{\max}^{3-D_p-D_t} - \bar{r}_{\min}^{3-D_p-D_t}\right] \tag{8}$$

In the above equation we set the constraint $3 - D_p - D_t > 0$ in order to allow small values of $\bar{r}_{\min}$.

2.2. Hydraulic conductivity

Fluid flux along each tube is typically obtained by solving Stokes equation in cylindrical coordinates. For a periodically varying aperture, it is assumed to be equal to that of a straight tube with constant radius $\bar{r}$ and equivalent permeability $k_e(\bar{r})$ given by Reis and Acock [61]:

$$k_e(\bar{r}) = \left[\frac{1}{l(\bar{r})} \int_0^{l(\bar{r})} \frac{8}{r^2(x)} dx\right]^{-1} \tag{9}$$

Substituting (1) in (9) and assuming $\lambda \ll l(\bar{r})$ (i.e. there are a large number of pore bodies and necks in a single pore) yields

$$k_e(\bar{r}) = \frac{\bar{r}^2}{8} (1 - 4a^2)^{3/2} \tag{10}$$

Then, the flux in a tube with periodically varying aperture can be expressed as:

$$q(\bar{r}) = \frac{\rho g}{\mu} k_e(\bar{r}) \frac{\Delta h}{l(\bar{r})} \tag{11}$$

where ρ is the water density, g gravity, μ water viscosity and Δh the head drop across the REV. Substituting (4) and (10) into (11) we obtain

$$q(\bar{r}) = \frac{(1 - 4a^2)^{3/2} \rho g}{8\mu} \bar{r}^{1+D_t} \frac{\Delta h}{L^{D_t}} \tag{12}$$

The total volumetric flow rate can be obtained by integrating (12) over the entire range of pore sizes:

$$\begin{aligned} Q &= \int_{\bar{r}_{\min}}^{\bar{r}_{\max}} q(\bar{r}) \pi \bar{r}^2 dN \\ &= \frac{(1 - 4a^2)^{3/2} \rho g \pi\, D_p \bar{r}_{\max}^{D_p}}{8\mu(3 + D_t - D_p)} \frac{\Delta h}{L^{D_t}} \left[\bar{r}_{\max}^{3+D_t-D_p} - \bar{r}_{\min}^{3+D_t-D_p}\right] \end{aligned} \tag{13}$$

On the basis of Darcy's law, total volumetric flow rate through the REV can be expressed as

$$Q = \pi R^2 K_s \frac{\Delta h}{L} \tag{14}$$

where K_s is the saturated hydraulic conductivity. Then, combining (13) and (14) we have

$$K_s = \frac{(1 - 4a^2)^{3/2} \rho g\, D_p \bar{r}_{\max}^{D_p}}{L^{D_t-1} R^2 8\mu(3 + D_t - D_p)} \left[\bar{r}_{\max}^{3+D_t-D_p} - \bar{r}_{\min}^{3+D_t-D_p}\right] \tag{15}$$

Similar equations have been derived by other authors. Possibly, the closest is the one by Karacan [62], if $(3 + D_t - D_p)$ in Eq. (15) is substituted by $(2.531 + D_t - D_p)$. The different exponent results from assuming that Eq. (8) needs to be modified for the shape of the pore.

Eq. (15) also yields the widely used dependence of permeability on a power of porosity [63] if $\bar{r}_{\min}$ is neglected, which leads to permeability proportional to $\phi^{(3+D_t)/(3-D_t)}$. This issue will be analyzed further when discussing the effect of dissolution. For now, it is interesting to notice that in this case the exponent does not depend on D_p and that the Kozeny equation is obtained for $D_t = 1.5$.

2.3. Diffusion coefficient

The concentration gradient along a single capillary tube with variable aperture can be obtained from Fick's law as:

$$\frac{dc}{dx} = \frac{J(\bar{r})}{D_{aq} \pi r^2(x)} \tag{16}$$

where D_{aq} is the aqueous diffusion coefficient, $J(\bar{r})$ is the diffusive solute mass flow rate and dc/dx is the solute concentration gradient. Integrating both sides along the pore length and rearranging terms yields:

$$J(\bar{r}) = -D_{aq}\left[\frac{1}{l(\bar{r})}\int_0^{l(\bar{r})}\frac{1}{\pi r^2(x)}dx\right]^{-1}\frac{\Delta c}{l(\bar{r})} \tag{17}$$

where Δc is the solute concentration difference between the edges of the tube.

Substituting (1) in (17) and assuming $\lambda \ll l(\bar{r})$ yields

$$J(\bar{r}) = -D_{aq}\pi\bar{r}^2(1-4a^2)^{3/2}\frac{\Delta c}{l(\bar{r})} \tag{18}$$

note that for $a = 0$ we obtain the diffusive mass flow rate of a straight tube or radius $\bar{r}$.

The total diffusive mass flow rate (J_t) through the rock sample is the sum of the flow rates of all individual tubes. According to (3) and (18) we have

$$\begin{aligned} J_t &= \int_{\bar{r}_{\min}}^{\bar{r}_{\max}} J(\bar{r})dN \\ &= -\frac{D_{aq}\pi(1-4a^2)^{3/2}D_p r_{\max}^{D_p}}{(1+D_t-D_p)}\frac{\Delta c}{L^{D_t}}\left[\bar{r}_{\max}^{1+D_t-D_p} - \bar{r}_{\min}^{1+D_t-D_p}\right] \end{aligned} \tag{19}$$

On the other hand, the total mass flow rate can be described by Fick's law

$$J_t = -D_{\text{eff}}\pi R^2\frac{\Delta c}{L} \tag{20}$$

where D_{eff} is the effective diffusion coefficient.

Combining (19) and (20) we obtain the following expression for the effective diffusion coefficient:

$$D_{\text{eff}} = D_{aq}\frac{(1-4a^2)^{3/2}D_p\bar{r}_{\max}^{D_p}}{(1+D_t-D_p)R^2L^{D_t-1}}\left[\bar{r}_{\max}^{1+D_t-D_p} - \bar{r}_{\min}^{1+D_t-D_p}\right] \tag{21}$$

Note that for $\bar{r}_{\min} \to 0$ the classical definition of D_{eff} [64] is obtained from (21):

$$D_{\text{eff}} = D_{aq}\frac{\phi}{\tau^2}f \tag{22}$$

where ϕ is the porosity given by (8), and τ and f are, respectively, tortuosity and constrictivity factors given by

$$\tau = \frac{l(\bar{r}_{\max})}{L} = \bar{r}_{\max}^{1-D_t}L^{D_t-1} \tag{23}$$

$$f = \frac{(1-4a^2)^{3/2}}{1+2a^2}\frac{3-D_p-D_t}{1+D_t-D_p} \tag{24}$$

Notice that this definition of constrictivity requires not only $3-D_p-D_t > 0$, but also $1+D_t-D_p > 0$.

2.4. Retention curve

As it is well-known, retention curves obtained from drainage and imbibition tests are different because of hysteresis phenomena, which are essential for some multiphase flow problems (e.g., [65]). The effect of hysteresis in saturation curves can be easily modeled with the sinusoidal pore geometry illustrated in Fig. 1 and described by Eq. (1). For this pore geometry, Czachor [59] derived an exact expression for the pressure head

$$\mathrm{h}(\mathrm{x_m}) = \frac{2\sigma}{\rho g\bar{r}}\frac{cos(\beta) - \frac{2\pi r'}{\lambda}\sin(\beta)cos(2\pi \mathrm{x_m}/\lambda)}{(1+2a\sin(2\pi \mathrm{x_m}/\lambda))\sqrt{1+\left[\frac{2\pi r'}{\lambda}\cos(2\pi \mathrm{x_m}/\lambda)\right]^2}} \tag{25}$$

where σ is the surface tension of the water, β the contact angle and $\mathrm{x_m}$ the position of wetting perimeter (meniscus). Under the assumption that the amplitude of the fluctuation r′ is much smaller than the wavelength λ, the above equation can be simplified to

$$\mathrm{h}(\mathrm{x_m}) = \frac{2\sigma cos(\beta)}{\rho g\bar{r}(1+2a\sin(2\pi \mathrm{x_m}/\lambda))} \tag{26}$$

Note that Eq. (26) is similar to the Young-Laplace equation for a straight capillary tube, except for the fact that the pressure head value changes with the position of the meniscus as $\mathrm{r}_h = \bar{r}(1+2a\sin(2\pi \mathrm{x_m}/\lambda))$.

To obtain the main drying saturation curve we suppose that the soil sample is initially fully water-saturated and is dewatered by a tension h. A tube becomes desaturated if suction h is smaller than that of Eq. (26). Otherwise, water will hang from the pore necks. The radius of each pore of the sample fluctuates between $\bar{r}(1-2a)$ and $\bar{r}(1+2a)$. Therefore it is reasonable to assume that pores with minimum radius $\bar{r}(1-2a) \geqslant r_h = 2\sigma cos(\beta)/\rho gh$ are drained by the tension h. Then, according to (3) and (6) the drying saturation is given by:

$$S^d(h) = \frac{\int_{\bar{r}_{\min}}^{r_h/(1-2a)} V_p dN}{\int_{\bar{r}_{\min}}^{\bar{r}_{\max}} V_p dN} = \frac{r_h^{3-D_p-D_t} - (\bar{r}_{\min}(1-2a))^{3-D_p-D_t}}{(\bar{r}_{\max}(1-2a))^{3-D_p-D_t} - (\bar{r}_{\min}(1-2a))^{3-D_p-D_t}} \tag{27}$$

Substituting (26) into (27) yields

$$S^d(h) = \begin{cases} 1 & h < h_{d,\min} \\ \frac{h^{D_p+D_t-3} - h_{d,\max}^{D_p+D_t-3}}{h_{d,\min}^{D_p+D_t-3} - h_{d,\max}^{D_p+D_t-3}} & h_{d,\min} \leqslant h \leqslant h_{d,\max} \\ 0 & h_{d,\min} < h \end{cases} \tag{28}$$

where

$$h_{d,\min} = \frac{2\sigma\cos(\beta)}{\rho g\bar{r}_{\max}(1-2a)} \quad h_{d,\max} = \frac{2\sigma\cos(\beta)}{\rho g\bar{r}_{\min}(1-2a)} \tag{29}$$

Similarly, the *main wetting saturation curve* can be derived assuming that the soil sample is initially dry and it is flooded with a tension h. In this case, only the tubes with maximum radii $\bar{r}(1+2a) \leqslant r_h$ will be fully saturated by water and the wetting saturation curve is given by:

$$S^w(h) = \begin{cases} 1 & h < h_{w,\min} \\ \frac{h^{D_p+D_t-3} - h_{w,\max}^{D_p+D_t-3}}{h_{w,\min}^{D_p+D_t-3} - h_{w,\max}^{D_p+D_t-3}} & h_{w,\min} \leqslant h \leqslant h_{w,\max} \\ 0 & h_{w,\min} < h \end{cases} \tag{30}$$

where

$$h_{w,\min} = \frac{2\sigma\cos(\beta)}{\rho g\bar{r}_{\max}(1+2a)} \quad h_{w,\max} = \frac{2\sigma\cos(\beta)}{\rho g\bar{r}_{\min}(1+2a)} \tag{31}$$

Scanning drying curves (i.e. if the regime shifts from wetting to drying) starting at tension $h_{1,d}$ are approximated by maintaining relative saturation constant until the tension increases to the value $h_{2,d}$ where $S^d(h_{2,d}) = S^w(h_{1,d})$.

Similarly, *scanning wetting curves* (i.e. if the regime shifts from drying to wetting) starting at tension $h_{1,w}$ are approximated by maintaining relative saturation constant until the tension decreases to the value $h_{2,w}$ where $S^w(h_{2,w}) = S^d(h_{1,w})$.

Note that Eqs. (28) and (30) have the same form as Perfect's model (Eq. (8) in [30]). The exponent is different because our model includes the fractal dimensions of pore size and tortuosity, whereas Perfect's considers a volumetric "prefractal" characterized by a single dimension D. The two equations are identical if $D = D_t + D_p$. Similar prefractal equations have been proposed by Rieu and Sposito [31] and Perrier et al. [32].

2.5. Unsaturated hydraulic conductivity

The *main drying unsaturated hydraulic conductivity* curve can be derived in a similar way as Eq. (28). During drainage only tubes

with minimum radius $\bar{r}(1-2a) \leqslant r_h$ are fully saturated. Then, if we neglect film flow on tube surfaces the main contribution to the total flow can be obtained as follows:

$$Q = \int_{\bar{r}_{min}}^{r_h/(1-2a)} q(\bar{r})\pi\bar{r}^2 dN \tag{32}$$

On the other hand, according to Buckingham–Darcy's law total volumetric flow rate through the REV can be expressed as

$$Q = \pi R^2 K(h)\frac{\Delta h}{L} \tag{33}$$

Finally, combining (32) and (33), and using (3), (12), (15), and (26) we obtain

$$K^d(h) = \begin{cases} K_s & h < h_{d,\min} \\ K_s \dfrac{h^{D_p-D_t-3} - h_{d,\max}^{D_p-D_t-3}}{h_{d,\min}^{D_p-D_t-3} - h_{d,\max}^{D_p-D_t-3}} & h_{d,\min} \leqslant h \leqslant h_{d,\max} \\ 0 & h_{d,\max} < h \end{cases} \tag{34}$$

Similarly, the main wetting unsaturated hydraulic conductivity curve pores is obtained by integrating (33) between $\bar{r}_{\min}$ and $r_h/(1+2a)$

$$K^w(h) = \begin{cases} K_s & h < h_{w,\min} \\ K_s \dfrac{h^{D_p-D_t-3} - h_{w,\max}^{D_p-D_t-3}}{h_{w,\min}^{D_p-D_t-3} - h_{w,\max}^{D_p-D_t-3}} & h_{w,\min} \leqslant h \leqslant h_{w,\max} \\ 0 & h_{w,\max} < h \end{cases} \tag{35}$$

Note that the exponent of h in Eqs. (34) and (35) is different from that in Eqs. (28) and (30).

Saturation curves (28) and (30), and hydraulic conductivity curves (34) and (35) have some similarities with the expressions of the well-known Brooks–Corey constitutive model, which are [26]

$$S(h) = \begin{cases} 1 & h < 1/a_{bc} \\ (a_{bc}h)^{-\gamma} & h \geqslant 1/a_{bc} \end{cases} \tag{36}$$

$$K(h) = \begin{cases} K_s & h < 1/a_{bc} \\ K_s(a_{bc}h)^{-(3\gamma+2)} & h \geqslant 1/a_{bc} \end{cases} \tag{37}$$

where a_{bc} is the reciprocal of air entry pressure and γ is a model parameter related to pore size distribution. Saturation relation (36) is an empirical expression while hydraulic conductivity (37) is obtained using the saturation relation in the Burdine model [66]. For $D_t = 2 - D_p/2$ (relation which is valid for the whole range of D_p values) and $\bar{r}_{\min} \to 0$, saturation curves (28) and (30) and hydraulic conductivity curves (34) and (35) are identical to the ones proposed by Brooks and Corey [26]. Under the above assumptions, the relations between parameters of both models are $a_{bc} = 1/h_{d,\min}$ and $a_{bc} = 1/h_{w,\min}$ for the main drying and wetting curves, respectively, and $\gamma = 1 - D_p/2$. According to the last relation, the range of value for the empirical parameter γ is (0,1) which is in agreement with the experimental data obtained by Rawls et al. [67] for the 11 USDA soil texture classes.

Scanning drying unsaturated hydraulic conductivity curves starting at tension $h_{1,d}$ are approximated by maintaining $K(h) = K(h_{1,d})$ until h has increased to $h_{2,d}$ determined in the section above; scanning wetting unsaturated hydraulic conductivity curves starting at tension $h_{1,w}$ are approximated by maintaining $K(h) = K(h_{1,w})$ until h has decreased to $h_{2,w}$.

2.6. Dissolution of the rock matrix

Dissolution rate can be transport or kinetically controlled, depending on whether the local reaction is fast or slow, respectively. As mentioned in the introduction, the objective of our model is to predict the changes of continuum macroscale properties in response to dissolution. In practice, this requires dissolution to be sufficiently slow at the discretization scale (cell or element), so that the cylindrical nature of the tubes is not affected by dissolution (this may require a fine discretization in regions where the fluids are very aggressive). The actual overall dissolution rate will be computed by the continuum model. Therefore, our goal here is not so much computing the dissolution rate as evaluating how it affects the pore structure. To this end, the local dissolution rate α is assumed to be function of the pore radius and the volume change of each pore is assumed to be proportional to the reactive area in contact with the reactive fluid:

$$\frac{dV_p(\bar{r})}{dt} = \alpha(\bar{r})S_p(\bar{r}) \tag{38}$$

where S_p is the surface of the tube. In general, dissolution will only occur at saturated pores. But for further developments, we assume that, similar to the film depositional model of Freedman et al. [41], dissolution affects pore radii of all tubes (i.e. the entire pore-size distribution). Therefore, according to (38) and (1), we obtain the following variation for the average radius

$$\frac{d\bar{r}}{dt} = \frac{2\alpha(\bar{r})}{(3-D_t)(1+2a^2)} \tag{39}$$

The key question is how to distribute the overall dissolution rate, computed by the continuum scale model, among the pore radii, that is, how to define $\alpha(\bar{r})$. The two extreme models would be: (i) to make the dissolution constant, which would reflect an extremely slow dissolution rate, independent of the actual dissolution along the flow path, or (ii) proportional to r^2, which would reflect a dissolution rate proportional to the flow rate. The latter may be appropriate for very aggressive dissolutions, leading to wormholes near the injection point, which would render our model inadequate, both because of pores coalescence and because non-uniform dissolution along the flow path. The former tends to unit fractal dimension, which does not seem appropriate, either, because, as pointed out by several authors (e.g., [68,69]), large pores grow faster than the small ones during dissolution processes. Therefore, we assumed dissolution rate proportional to pore radius, which falls between the two extrema, and it is convenient (fractal dimension remains unaffected) and consistent with a mild transport control on dissolution kinetics. Therefore, $\alpha(\bar{r}) = \tilde{\alpha}\bar{r}$, where $\tilde{\alpha}$ will generally be obtained at every cell to reproduce the overall dissolution computed by the continuum model, but is assumed constant here for evaluating the time evolution of controlling parameters. Integrating (39) from t_0 (initial time for dissolution) to t, we obtain

$$\bar{r}(t) = \bar{r}(t_0)e^{\beta(t-t_0)} \tag{40}$$

$$\beta = \frac{2\tilde{\alpha}}{(3-D_t)(1+2a^2)} \tag{41}$$

Substituting (41) in (8), (15), and (21):

$$\phi(t) = \phi(t_0)e^{(3-D_t)\beta(t-t_0)} \tag{42}$$

$$K_s(t) = K_s(t_0)e^{(3+D_t)\beta(t-t_0)} \tag{43}$$

$$D_{eff}(t) = D_{eff}(t_0)e^{(1+D_t)\beta(t-t_0)} \tag{44}$$

The saturation curves (28) and (30) and the unsaturated hydraulic conductivity curves (34) and (35) also depend on time through parameters defined in (29) and (31):

$$h_{d,\min}(t) = h_{d,\min}(t_0)e^{-\beta(t-t_0)}, \quad h_{d,\max}(t) = h_{d,\max}(t_0)e^{-\beta(t-t_0)} \tag{45}$$

$$h_{w,\min}(t) = h_{w,\min}(t_0)e^{-\beta(t-t_0)}, \quad h_{w,\max}(t) = h_{w,\max}(t_0)e^{-\beta(t-t_0)} \tag{46}$$

Note that combining (42) and (43) we obtain a commonly used correlation for estimating permeability evolution [63]:

$$K_s(t) = K_s(t_0)\left(\frac{\phi(t)}{\phi(t_0)}\right)^n \tag{47}$$

with $n = (3 + D_t)/(3 - D_t)$. According to Aharonov et al. [70] the exponent n is a constant usually 2 or greater; the well-known cubic law is consistent with $n = 3$, and Doyen [63] suggested that the best fit of data in their study is obtained using $n = 3.8$. Note that in the proposed model the exponent n only depends on the tortuosity fractal dimension D_t, so the range of this parameter is $2 < n < 5$. The value of Doyen [63] would lead to $D_t = 1.75$.

3. Application

Actual application of the model requires specifying the pore size and tortuosity fractal dimensions, the minimum and maximum pore radii, as well as the fluctuation parameter, a, and the REV. Most of these parameters can be obtained from pore image analysis and, hopefully, others (e.g., tortuosity dimension) can be borrowed from experiments in similar media, once experience has been gained. To this end, it would be desirable to get experimental data sets from laboratory experiments that yield the evolution of porosity, saturated and relative permeabilities, retention curve, and diffusion coefficient during dissolution. We performed a review of published data, but we did not find any. Therefore, for illustration purposes, we present here the fit to porosity and saturated permeability evolutions presented by Jove Colon et al. [71], Békri et al. [68] and Rötting et al. [72].

Jove Colon et al. [71] studied the evolution of saturated permeability and porosity during dissolution of nonfractured, clay-free Fontainebleau sandstone at 80 °C and far from equilibrium conditions using a 0.1 M NaOH. To test our model at least partially, we applied it to the data of core 1 in the publication [71].

In order to fit the proposed model to the observational data we use an exhaustive search method, which is a simple and very robust technique to find the best set of model parameters. To apply this method, we first define the ranges of admissible values for each model parameter and uniformly discretize the space of parameters. The exhaustive search method computes the error between data and predicted values for all possible combinations of model parameters values and selects the ones that minimize the error. Figs. 2 and 3 show the fit of expressions (42) and (43). The values of fitted parameters are: $a = 0.025$, $D_p = 1.05$, $D_t = 1.80$, $\tilde{\alpha} = 1.4125\,10^{-4}$, $\bar{r}_{\min} = 3.98\ 10^{-6}$ cm, and $\bar{r}_{\max} = 0.01$ cm. The latter is qualitatively consistent with the photomicrograph of the core shown by Jove Colon et al. [71]. It is worth pointing that the above set of parameters produces the best fit to observational data assuming a wide range of admissible values for all model parameters. Clearly, fitting the model requires further information either on parameter distributions or on the evolution of other variables of the problem.

The proposed model is also tested with simulated data obtained by Békri et al. [68]. In their study the dissolution phenomena is described at microscopic scale by a coupled convection and convection-diffusion problem in the quasi-steady limit, where the geometrical changes are very slow. Using this approach they numerically compute the evolution of the permeability in a close-packed cubic array of spheres. Figs. 4 and 5 show the fit of expressions (43) and (47) to simulated values of the normalized permeability with dimensionless time and normalized porosity for small values of the product of the Péclet and Damköhler numbers (uniform dissolution). The best agreement between simulated values and our model is obtained for $a = 0.165$, $\tilde{\alpha} = 1.036$,

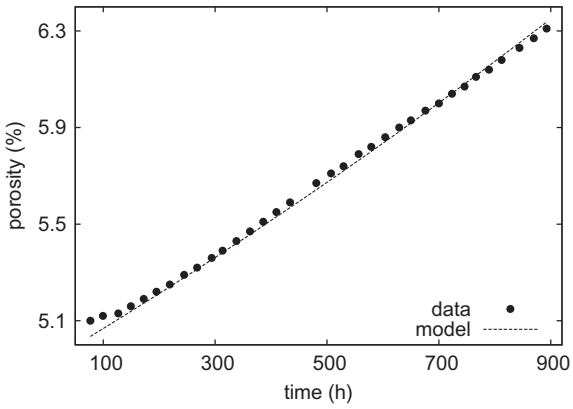

Fig. 2. Model fit to the time evolution of porosity data obtained by Jove et al. [71].

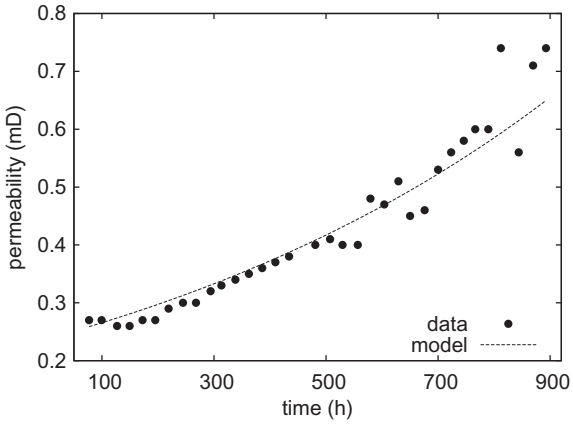

Fig. 3. Model fit to the time evolution of permeability data obtained by Jove et al. [71].

$D_t = 1.83$, which are the only parameters that can be estimated because data are normalized by the initial values.

It is interesting to point out that the values of the tortuosity dimension obtained in both cases (around 1.8) are similar to the value derived from the data of Doyen [63]. They yield an exponent of approximately $n = 4$ in the relationship $K_s(t)$ vs. $\phi(t)$ of Eq. (47).

Finally, we applied the model to laboratory data recently obtained by the authors and co-workers [72] on dolomitized oolitic grainstones from the Campos basin in Majorca. Before and after attacks with HCl at pH 4, we determined the porosity (by triple

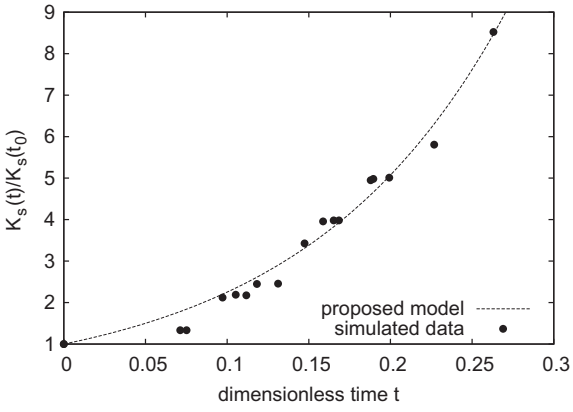

Fig. 4. Model fit to the time evolution of permeability presented by Békri et al. [68].

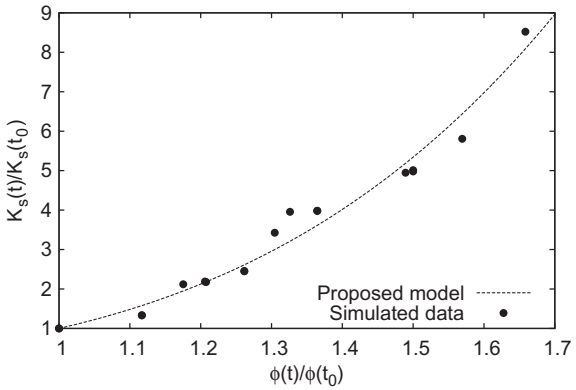

Fig. 5. Model fit to the permeability versus porosity data presented by Békri et al. [68].

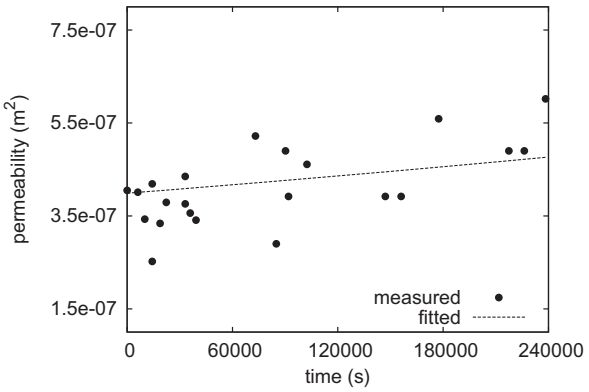

Fig. 7. Model fit to time evolution of permeability data measured by Rötting et al. [72].

weighing) and the main drying saturation curve (by centrifuge). We also attempted to measure diffusion coefficients, but the initial permeability of the core was too high (about 2 cm/min or $4 \cdot 10^{-11}$ m^2) to produce pure diffusion without any advective or convective interference. Three characterization and two dissolution steps were performed, with a total percolated acid volume of 17,100 pore volumes, at a flow rate of 10 mL/min. The cylindrical core had a diameter of 25 mm and a thickness of 12 mm, which gives an upper bound for the radius R and defines the length L of the REV. A maximum grain size of about 0.2 mm and maximum pore diameters of about 0.4 mm were determined from thin sections, the latter provides an upper limit for the maximum average pore radius $\bar{r}_{max}$. A residual water content of about 5% at the highest centrifuge speed (equivalent tension 213 kPa) indicated that the minimum pore radius $\bar{r}_{min}$ was 0.0005 mm or smaller. Further details about these experiments can be found elsewhere [72].

This data set allowed us to also test the drying saturation relationship (28) and (29) and its time evolution (45), besides the evolution of porosity and permeability (Eqs. (42) and (43)). We used a water viscosity $\mu = 0.001$ Pa · s, a water density $\rho = 1000$ kg/m^3, a surface tension $\sigma = 0.072$ N/m and a contact angle $\beta = 0°$. The remaining parameters adjusted by the exhaustive search method are: $R = 7.610^{-2}$ cm, $a = 0.001$, $D_p = 1.123$, $D_t = 1.266$, $\bar{r}_{min} = 9.2 \cdot 10^{-8}$ cm, $\bar{r}_{max} = 1.98 \cdot 10^{-2}$ cm and $\tilde{\alpha} = 1.5 \cdot 10^{-7}$.

The fit of the model to porosity and permeability evolution, and to three measured drying saturation curves at $t = 0$ s, 33,095 s and 238,307 s are shown in Figs. 6–8, respectively.

An excellent fit is obtained for the porosity evolution (Fig. 6), good fits for permeability evolution (Fig. 7) and drying saturation

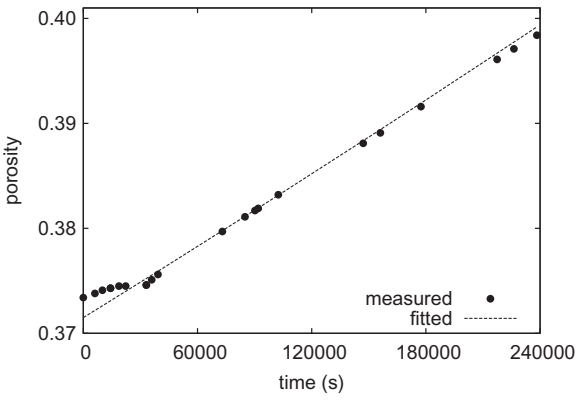

Fig. 6. Model fit to time evolution of porosity data measured by Rötting et al. [72].

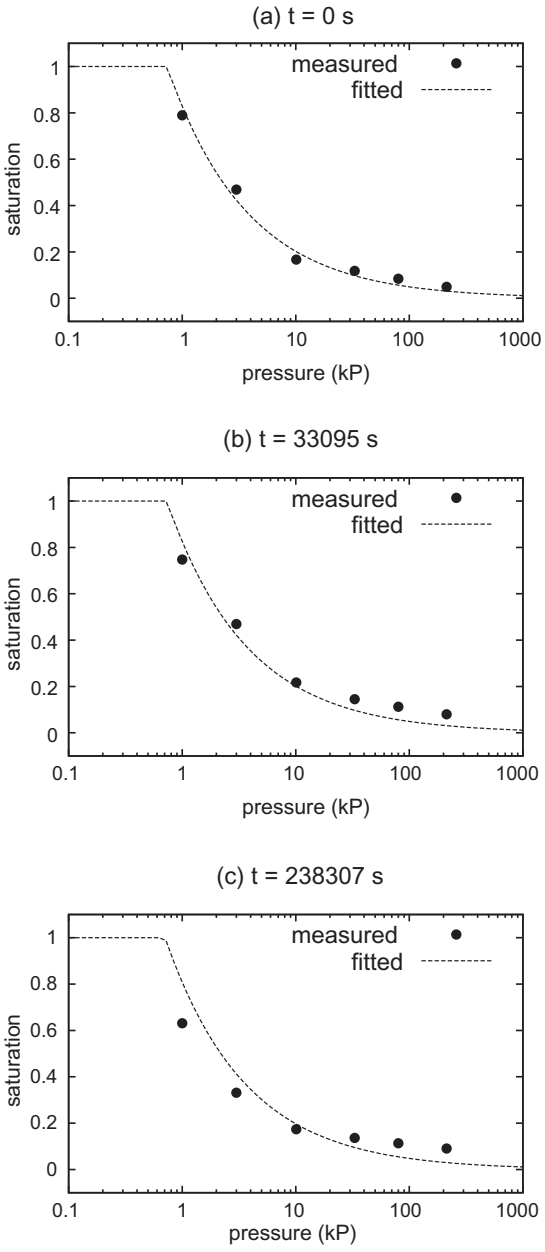

Fig. 8. Model fit to primary drainage saturation relations at $t = 0$ s (a), $t = 33{,}095$ s (b) and $t = 238{,}307$ s (c) measured by Rötting et al. [72].

relations (Fig. 8). The final drying saturation relation (t = 238,307 s) is reproduced less satisfactorily, particularly for low tensions (large pore sizes). Probably, dissolution decreased the tortuosity, changing its fractal dimension D_t and the fluctuation ratio a, because dissolution may have enlarged the pore necks more than the pore bodies. Such changes cannot be reproduced by the model proposed here, because the fractal dimensions of tortuosity D_t and porosity D_p are supposed to remain constant during dissolution. Experiments would need to be performed in a chemical system with much slower dissolution velocities than dolomite and HCl, in order to achieve a more uniform dissolution of the porous medium.

With the values of D_t = 1.266 obtained with this dataset, the exponent in the relationship $K_s(t)$ vs. $\phi(t)$ of Eq. (47) yields n = 2.46, significantly lower than in the previous two cases.

4. Discussion and conclusions

A physically-based theoretical model for describing the temporal evolution of porosity, saturated and relative permeabilities, retention curve, and diffusion coefficient during rock dissolution by reactive fluids has been developed in this study. The derivation of the model is based on the assumption that the porosity of the rock can be represented by a bundle of tortuous capillary tubes with a sinusoidal variation of tube radius along the tube length and a fractal cumulative size distribution for the mean radius. Using fractal descriptions of the pore size distribution and tortuosity, analytical expressions were obtained that depend only on the minimum and maximum pore radii, the size of the representative elemental volume and the fractal dimensions of pore size and tortuosity. By assuming periodic fluctuations in the radius of the pores, hysteresis in the retention curve and in the relative permeability function was represented. Assuming a constant dissolution reaction, closed-form analytical expressions for porosity, retention curve, saturated and relative permeabilities and diffusion were obtained that depend explicitly on time.

We show for most of the derived equations that under simplifying conditions the expressions are equivalent to widely used empirical relations, such as Kozeny-Carman [4,5], Brooks and Corey [26], Campbell [35], fractal models derived by others (e.g. [30–32]), or commonly used equations of the effective diffusion coefficient or the evolution of permeability as an exponential function of porosity [63,70].

The proposed model represents an improvement over available bundles of tubes models in that it blends existing concepts (fractal tortuosity and pore sizes, and constrictivity), to obtain an integrated description of multiphase flow properties and how they evolve in response to rock dissolution. However, the proposed model suffers the limitations of bundles of tubes approaches. Specifically, they assume perfect pore connectivity and stationary pore structure. As a result, they cannot account for non-stationary features such as lacunarity. This limitation can be partly overcome by specifying multiple interacting continua. Such specification is not needed by pore network models, but results from pore geometry and pore scale processes. Therefore it is clear that these must be considered to be more realistic than bundles of tubes, provided that good pore images are available [12].

The proposed equations can be enriched along several directions. First, for simplicity and convenience, we assumed dissolution to occur in all pores. In general, it will only occur in saturated pores. Accounting for this will require keeping track to the evolution of pore size distribution, which may no longer be fractal. Also, dissolution and precipitation may not be uniform along the tubes, but concentrate preferentially on the pore necks or bodies. In fact, the uniform distribution of pore sizes along the tubes may have to be relaxed to better reproduce hysteresis phenomena.

The temporal evolution predicted by the proposed model for porosity and permeability compares well with data published by Jove Colon et al. [71] and by Békri et al. [68]. We are currently performing laboratory experiments to test the model against temporal evolution of not only porosity and permeability, but also molecular diffusion and retention curve. A first test of our model with data from one of these experiments [72] also gave a good fit for porosity and permeability evolution, and saturation relations.

Acknowledgements

This study was partly funded by the PANACEA project (European Commission FP7 contract no. 282900, www.panacea-co2.org), and by CONICET (Argentina). The authors wish to thank Behzad Ghanbarian and four anonymous reviewers for their careful assessment of our work and the very detailed, constructive comments that helped to greatly improve the quality of the manuscript.

References

[1] Parmigiani A, Huber C, Bachmann O, Chopard B. Pore-scale mass and reactant transport in multiphase porous media flows. J Fluid Mech 2011;686:40–76. http://dx.doi.org/10.1017/jfm.2011.268.
[2] Saripalli KP, Meyer PD, Bacon DH, Freedman VL. Changes in hydrologic properties of aquifer media due to chemical reactions: a review. Crit Rev Environ Sci Technol 2001;31:311–49. http://dx.doi.org/10.1080/20016491089244.
[3] Bernabe Y, Mok U, Evans B. Permeability-porosity relationships in rocks subjected to various evolution processes. Pure Appl Geophys 2003;160:937–60. http://dx.doi.org/10.1007/pl00012574.
[4] Kozeny J. Über kapillare leitung des wassers im boden. Sitzungsber Akad Wiss 1927;136:271–306.
[5] Carman PC. Fluid flow through granular beds. Trans Inst Chem Eng 1937;15:150–66.
[6] Pape H, Clauser C, Iffland J. Permeability prediction based on fractal pore-space geometry. Geophysics 1999;64:1447–60. http://dx.doi.org/10.1190/1.1444649.
[7] Civan F. Scale effect on porosity and permeability: kinetics, model, and correlation. Aiche J 2001;47:271–87. http://dx.doi.org/10.1002/aic.690470206.
[8] Bourbie T, Zinszner B. Hydraulic and acoustic properties as a function of porosity in Fontainebleau sandstone. J Geophys Res Solid Earth Planets 1985;90:1524–32. http://dx.doi.org/10.1029/JB090iB13p11524.
[9] Noiriel C, Gouze P, Bernard D. Investigation of porosity and permeability effects from microstructure changes during limestone dissolution. Geophys Res Lett 2004;31. http://dx.doi.org/10.1029/2004gl021572.
[10] Chapuis RP, Aubertin M. On the use of the Kozeny–Carman equation to predict the hydraulic conductivity of soils. Can Geotech J 2003;40:616–28. http://dx.doi.org/10.1139/t03-013.
[11] Sahimi M. Applications of percolation theory. London: CRC Press, Taylor & Francis; 1994.
[12] Blunt MJ, Bijeljic B, Dong H, Gharbi O, Iglauer S, Mostaghimi P, et al. Pore-scale imaging and modelling. Adv Water Resour 2013;51:197–216. http://dx.doi.org/10.1016/j.advwatres.2012.03.003.
[13] Berkowitz B, Ewing R. Percolation theory and network modeling applications in soil physics. Surv Geophys 1998;19:23–72. http://dx.doi.org/10.1023/a:1006590500229.
[14] Meakin P, Tartakovsky AM. Modeling and simulation of pore-scale multiphase fluid flow and reactive transport in fractured and porous media. Rev Geophys 2009;47. http://dx.doi.org/10.1029/2008rg000263.
[15] Tartakovsky AM, Meakin P, Scheibe TD, Wood BD. A smoothed particle hydrodynamics model for reactive transport and mineral precipitation in porous and fractured porous media. Water Resour Res 2007;43:18. http://dx.doi.org/10.1029/2005wr004770.
[16] Sahimi M, Gavalas GR, Tsotsis TT. Statistical and continuum models of fluid-solid reactions in porous media. Chem Eng Sci 1990;45:1443–502. http://dx.doi.org/10.1016/0009-2509(90)80001-U.
[17] Kang QJ, Tsimpanogiannis IN, Zhang DX, Lichtner PC. Numerical modeling of pore-scale phenomena during CO_2 sequestration in oceanic sediments. Fuel Process Technol 2005;86:1647–65.
[18] Tartakovsky AM, Redden G, Lichtner PC, Scheibe TD, Meakin P. Mixing-induced precipitation: experimental study and multiscale numerical analysis. Water Resour Res 2008;44. http://dx.doi.org/10.1029/2006wr005725.
[19] Scheibe TD, Tartakovsky AM, Tartakovsky DM. Redden GD, Meakin P. Hybrid numerical methods for multiscale simulations of subsurface biogeochemical processes. In: SciDac 2007: scientific discovery through advanced computing, 2007. p. U487–91.
[20] Varloteaux C, Békri S, Adler PM. Pore network modelling to determine the transport properties in presence of a reactive fluid: from pore to reservoir

scale. Adv Water Resour 2013;53:87–100. http://dx.doi.org/10.1016/j.advwatres.2012.10.004.
[21] Rhodes ME, Bijeljic B, Blunt MJ. Pore-to-field simulation of single-phase transport using continuous time random walks. Adv Water Resour 2008;31:1527–39. http://dx.doi.org/10.1016/j.advwatres.2008.04.006.
[22] Tartakovsky AM, Tartakovsky DM, Scheibe TD, Meakin P. Hybrid simulations of reaction-diffusion systems in porous media. Siam J Sci Comput 2008;30:2799–816. http://dx.doi.org/10.1137/070691097.
[23] Zhu J, Ma J. An improved gray lattice Boltzmann model for simulating fluid flow in multi-scale porous media. Adv Water Resour 2013;56:61–76. http://dx.doi.org/10.1016/j.advwatres.2013.03.001.
[24] Lichtner PC, Kang Q. Upscaling pore-scale reactive transport equations using a multiscale continuum formulation. Water Resour Res 2007;43:W12S5. http://dx.doi.org/10.1029/2006WR005664.
[25] Gouze P, Melean Y, Le Borgne T, Dentz M, Carrera J. Non-Fickian dispersion in porous media explained by heterogeneous microscale matrix diffusion. Water Resour Res 2008;44. http://dx.doi.org/10.1029/2007wr006690.
[26] Brooks RH, Corey AT. Hydraulic properties of porous media. Hydrology Papers 3. Colorado State University; Fort Collins, CO: 1964. p. 37.
[27] Childs EC, Collis-George N. The permeability of porous materials. Proc R Soc London Ser A 1950;201:392–405. http://dx.doi.org/10.1098/rspa.1950.0068.
[28] Mualem Y. New model for predicting hydraulic conductivity of unsaturated porous-media. Water Resour Res 1976;12:513–22. http://dx.doi.org/10.1029/WR012i003p00513.
[29] van Genuchten MT. A closed-form equation for predicting the hydraulic conductivity of unsaturated soils. Soil Sci Soc Am J 1980;44:892–8.
[30] Perfect E. Estimating soil mass fractal dimensions from water retention curves. Geoderma 1999;88:221–31. http://dx.doi.org/10.1016/s0016-7061(98)00128-1.
[31] Rieu M, Sposito G. Fractal fragmentation, soil porosity, and soil water properties: 1. Theory. Soil Sci Soc Am J 1991;55:1231–8.
[32] Perrier E, Rieu M, Sposito G, de Marsily G. Models of the water retention curve for soils with a fractal pore size distribution. Water Resour Res 1996;32:3025–31. http://dx.doi.org/10.1029/96wr01779.
[33] Tyler SW, Wheatcraft SW. Fractal processes in soil-water retention. Water Resour Res 1990;26:1047–54. http://dx.doi.org/10.1029/90wr00034.
[34] Mandelbrot BB. The fractal geometry of nature. New York: W.H. Freeman; 1982.
[35] Campbell GS. Simple method for determining unsaturated conductivity from moisture retention data. Soil Sci 1974;117:311–4.
[36] Guarracino L. A fractal constitutive model for unsaturated flow in fractured hard rocks. J Hydrol 2006;324:154–62. http://dx.doi.org/10.1016/j.jhydrol.2005.10.004.
[37] Monachesi L, Guarracino L. A fractal model for predicting water and air permeabilities of unsaturated fractured rocks. Transp Porous Media 2011;90:779–89. http://dx.doi.org/10.1007/s11242-011-9815-9.
[38] Gimenez D, Perfect E, Rawls WJ, Pachepsky Y. Fractal models for predicting soil hydraulic properties: a review. Eng Geol 1997;48:161–83. http://dx.doi.org/10.1016/s0013-7952(97)00038-0.
[39] Ghanbarian-Alavijeh B, Millan H, Huang G. A review of fractal, prefractal and pore-solid-fractal models for parameterizing the soil water retention curve. Can J Soil Sci 2011;91:1–14. http://dx.doi.org/10.4141/cjss10008.
[40] Bartels J, Clauser C, Kuehn M, Pape H, Schneider W. Reactive flow and permeability prediction – numerical simulation of complex hydrogeothermal problems. In: Petrophysical properties of crystalline rocks, vol. 24, 2005. p. 133–51. doi: http://dx.doi.org/10.1144/GSL.SP.2005.240.01.11.
[41] Freedman VL, Bacon DH, Saripalli KP, Meyer PD. A film depositional model of permeability for mineral reactions in unsaturated media. Vadose Zone J 2004;3:1414–24.
[42] Wissmeier L, Barry DA. Effect of mineral reactions on the hydraulic properties of unsaturated soils: model development and application. Adv Water Resour 2009;32:1241–54. http://dx.doi.org/10.1016/j.advwatres.2009.05.004.
[43] Hillel D. Fundamentals of soil physics. New York: Academic Press Inc.; 1980.
[44] Mualem Y, Beriozkin A. General scaling rules of the hysteretic water retention function based on Mualem's domain theory. Eur J Soil Sci 2009;60:652–61. http://dx.doi.org/10.1111/j.1365-2389.2009.01130.x.
[45] Pham HQ, Fredlund DG, Barbour SL. A study of hysteresis models for soil-water characteristic curves. Can Geotech J 2005;42:1548–68. http://dx.doi.org/10.1139/t05-071.
[46] Izady A, Ghahraman B, Davari K. Hysteresis: phenomenon and modeling in soil-water relationship. Iran Agric Res 2009;28. Available online at: http://www.shirazu.ac.ir/files/extract_file.php?file_id=2549&ei=b2mqt9k-pomg0qwar_wiba&usg=afqjcngehwjlo3paxmaji2zbejqo68_a9q&sig2=v-ex9x4u3wo8pnpeix3nxg (last visited 9 May 012).
[47] Russell AR, Buzzi O. A fractal basis for soil-water characteristics curves with hydraulic hysteresis. Geotechnique 2012;62:269–74. http://dx.doi.org/10.1680/geot.10.P.119.
[48] Ojeda G, Perfect E, Alcaniz JM, Ortiz O. Fractal analysis of soil water hysteresis as influenced by sewage sludge application. Geoderma 2006;134:386–401. http://dx.doi.org/10.1016/j.geoderma.2006.03.011.
[49] Perfect E. Modeling the primary drainage curve of prefractal porous media. Vadose Zone J 2005;4:959–66. http://dx.doi.org/10.2136/vzj2005.0012.
[50] Bear J. Dynamics of fluids in porous media. New York: American Elsevier Pub. Co.; 1972.
[51] Lerman A. Geochemical processes – water and sediment environments. New York: Wiley-Interscience; 1979.
[52] Archie GE. The electrical resistivity log as an aid in determining some reservoir characteristics. Trans AIME 1942;146:54–62.
[53] Boving TB, Grathwohl P. Tracer diffusion coefficients in sedimentary rocks: correlation to porosity and hydraulic conductivity. J Contam Hydrol 2001;53:85–100.
[54] Liu J-g, Nie Y-f. Fractal scaling of effective diffusion coefficient of solute in porous media. J Environ Sci 2001;13:170–2.
[55] Hayek M, Kosakowski G, Churakov S. Exact analytical solutions for a diffusion problem coupled with a precipitation-dissolution reaction and feedback of porosity change. Water Resour Res 2011;47:13. http://dx.doi.org/10.1029/2010wr010321.
[56] Saripalli KP, Serne RJ, Meyer PD, McGrail BP. Prediction of diffusion coefficients in porous media using tortuosity factors based on interfacial areas. Ground Water 2002;40:346–52. http://dx.doi.org/10.1111/j.1745-6584.2002.tb02512.x.
[57] Yu BM, Li JH. Some fractal characters of porous media. Fractals-Complex Geometry Patterns and Scaling in Nature and Society. 2001;9:365–72. http://dx.doi.org/10.1142/s0218348x01000804.
[58] Yu BM, Li JH, Li ZH, Zou MQ. Permeabilities of unsaturated fractal porous media. Int J Multiphase Flow 2003;29:1625–42. http://dx.doi.org/10.1016/s0301-9322(03)00140-x.
[59] Czachor H. Modelling the effect of pore structure and wetting angles on capillary rise in soils having different wettabilities. J Hydrol 2006;328:604–13. http://dx.doi.org/10.1016/j.jhydrol.2006.01.003.
[60] Wheatcraft SW, Tyler SW. An explanation of scale-dependent dispersivity in heterogeneous aquifers using concepts of fractal geometry. Water Resour Res 1988;24:566–78. http://dx.doi.org/10.1029/WR024i004p00566.
[61] Reis JC, Acock AM. Permeability reduction models for the precipitation of inorganic solids in Berea sandstone. In Situ 1994;18:347–68.
[62] Karacan CÖ. Prediction of porosity and permeability of caved zone in longwall gobs. Transp Porous Media 2010;82:413–39. http://dx.doi.org/10.1007/s11242-009-9437-7.
[63] Doyen PM. Permeability, conductivity, and pore geometry of sandstone. J Geophys Res Solid Earth Planets 1988;93:7729–40. http://dx.doi.org/10.1029/JB093iB07p07729.
[64] van Brakel J, Heertjes PM. Analysis of diffusion in macroporous media in terms of a porosity, a tortuosity and a constrictivity factor. Int J Heat Mass Transfer 1974;17:1093–103. http://dx.doi.org/10.1016/0017-9310(74)90190-2.
[65] Juanes R, Spiteri EJ, Orr Jr FM, Blunt MJ. Impact of relative permeability hysteresis on geological CO_2 storage. Water Resour Res 2006;42. http://dx.doi.org/10.1029/2005wr004806.
[66] Burdine NT. Relative permeability calculation from pore-size distribution data. Petr Trans Am Inst Min Metall Eng 1953;198:71–7.
[67] Rawls WJ, Brakensiek DL, Saxton KE. Estimation of soil water properties. Trans Am Soc Agric Eng 1982;25(5):1316–28.
[68] Békri S, Thovert JF, Adler PM. Dissolution of porous media. Chem Eng Sci 1995;50:2765–91. http://dx.doi.org/10.1016/0009-2509(95)00121-K.
[69] Schechter RS, Gidley JL. The change in pore size distribution from surface reactions in porous media. AIChE J 1969;15:339–50. http://dx.doi.org/10.1002/aic.690150309.
[70] Aharonov E, Tenthorey E, Scholz CH. Precipitation sealing and diagenesis – 2. Theoretical analysis. J Geophys Res Solid Earth 1998;103:23969–81. http://dx.doi.org/10.1029/98jb02230.
[71] Jove Colon CF, Oelkers EH, Schott J. Experimental investigation of the effect of dissolution on sandstone permeability, porosity, and reactive surface area. Geochim. Cosmochim. Acta. 2004;68:805–17. http://dx.doi.org/10.1016/j.gca.2003.06.002.
[72] Rötting TS, Luquot L, Casalinuovo D, Carrera J. Joint evolution of porosity, permeability, water retention curve and reactive surface area during carbonate rock dissolution. Submitted to Chemical Geology.